The Astrophysical Journal, 580:1030–1042, 2002 December 1

EVIDENCE FOR HARMONIC RELATIONSHIPS IN THE HIGH-FREQUENCY QUASI-PERIODIC OSCILLATIONS OF XTE J1550−564 AND GRO J1655−40

Ronald A. Remillard and Michael P. Muno
Center for Space Research, Massachusetts Institute of Technology, Cambridge, MA 02139; rr@space.mit.edu, muno@space.mit.edu

Jeffrey E. McClintock
Harvard-Smithsonian Center for Astrophysics, 60 Garden Street, Cambridge, MA 02138; jem@cfa.harvard.edu

and

Jerome A. Orosz
Astronomical Institute, Utrecht University, Postbus 80000, 3508 TA Utrecht, The Netherlands; j.a.orosz@astro.uu.nl
Received 2002 February 4; accepted 2002 July 30

ABSTRACT

We continue to investigate the X-ray properties of the black hole binary XTE J1550−564. By grouping observations (1998–1999) according to the type of low-frequency quasiperiodic oscillation (LFQPO) identified in a previous paper, we show evidence that two high-frequency QPOs (HFQPOs) occur simultaneously near 184 and 276 Hz. We can model the QPO profiles while assuming that the central frequencies are related by a 3 : 2 ratio. In one group, there is some evidence of a broad feature at the fundamental frequency of 92 Hz. We also investigate the 2000 April outburst, and we confirm the suggestion of Miller et al. that a 270 Hz QPO is accompanied by a second feature near 180 Hz. The histogram for the 28 individual HFQPO detections in XTE J1550−564 shows two peaks near 184 and 276 Hz, while there is a notable exception in the 143 Hz QPO detected on 1998 October 15. Similarly, all of the 13 HFQPO detections in the black hole binary GRO J1655−40 occur at two frequencies that are related by a 3 : 2 ratio. We next investigate all of the energy spectra for XTE J1550−564, and we find a systematic increase in the strength of the power-law component as the stronger of the two HFQPOs shifts from 276 to 184 Hz. A strikingly similar result is seen in the spectra of GRO J1655−40 when the stronger HFQPO shifts from 450 to 300 Hz. The fundamental HFQPO frequencies for the two X-ray sources scale as M^{-1}, which is consistent with the hypotheses that these HFQPOs represent some kind of oscillation rooted in general relativity (GR) and that the two black holes have similar values of the dimensionless spin parameter. We discuss physical mechanisms that may explain these HFQPOs. A resonance between orbital and radial coordinate frequencies is one possibility suggested by Abramowicz & Kluzniak. For XTE J1550−564, this would imply moderate values for the dimensionless spin parameter ($0.1 < a_* < 0.6$), with similar results for GRO J1655−40. A resonance between polar and radial coordinate frequencies allows additional values for a_* above 0.9. There remain serious uncertainties regarding the physical mechanism whereby resonances in coordinate frequencies may produce HFQPOs. We also discuss models for "diskoseismic" oscillations. In this case, the concept that the inner disk behaves as a resonance cavity in GR has certain attractions for explaining HFQPOs, but integral harmonics are not predicted for the three types of diskoseismic modes derived for adiabatic perturbations in a thin accretion disk.

Subject headings: black hole physics — stars: individual (GRO J1655−40, XTE J1550−564) — stars: oscillations — X-rays: stars

1. INTRODUCTION

XTE J1550−564 is a recurrent X-ray nova and a microquasar that has been extensively studied at X-ray and optical frequencies. A major outburst during 1998–1999 revealed complex evolution in both its spectral properties and variability characteristics (Wijnands, Homan, & van der Klis 1999; Sobczak et al. 2000b; Homan et al. 2001; Remillard et al. 2002). It is one of five black hole candidates that exhibit transient high-frequency quasi-periodic oscillations (HFQPOs), while its stronger and more common low-frequency QPOs (LFQPOs) are seen to vary in frequency in response to changes in the spectrum of the accretion disk. Additional X-ray outbursts with weaker maxima and shorter duration were observed in 2000 April–June (Tomsick et al. 2001b; Miller et al. 2001), in 2001 February–March (Tomsick, Corbel, & Kaaret 2001a), and again in 2002 January (Swank, Smith, & Markwardt 2002). The accumulated investment of almost 400 *RXTE* pointed observations (2–200 keV) provides a unique archive of high-quality monitoring data that span four decades in X-ray luminosity, with several excursions through each of the canonical emission states of black hole binaries. These resources motivate continuing efforts to understand the structure of the accretion flow at various levels of X-ray luminosity and to search for effects of general relativity (GR) in the innermost regions of the accretion disk.

Optical photometry of XTE J1550−564 during outbursts revealed the binary period of 1.54 days and the perplexing weakness of an optical response to X-ray flares (Jain et al. 2001). Optical spectroscopy and photometry during accretion quiescence have recently established that the system is a dynamical black hole binary with a black hole mass of $10.0 \pm 1.5\ M_\odot$ (Orosz et al. 2002). The companion star is a late-type subgiant (G8 IV–K4 III), and the binary inclination angle is constrained to the range $72^\circ \pm 5^\circ$ (Orosz et al. 2002).

Radio observations revealed a relativistic jet associated with the large X-ray flare of 1998 September 19 (Hannikainen et al. 2001). The radio source then decayed

away while the X-ray source remained in the "very high" state. During the X-ray "low-hard" state seen in the outburst of 2000, weaker radio flux was detected with an inverted spectrum, suggesting the presence of a steady jet (Corbel et al. 2001).

In a previous paper (Remillard et al. 2002, hereafter RSMM02) we used 209 *RXTE* observations of XTE J1550−564 during its 1998–1999 outburst to investigate the relationships between HFQPOs, LFQPOs, and the spectral characteristics reported by Sobczak et al. (2000b). It was found that complex LFQPOs are better organized in their correlations with both HFQPOs and the accretion disk flux and temperature when we distinguished three types (A, B, and C) on the basis of phase lags and coherence values measured at the central QPO frequency. The LFQPO types (but not their frequencies) are correlated with the frequencies of HFQPOs that were detected on 20 occasions. Type A LFQPOs (5–10 Hz, broad profiles, lag in soft X-rays) are associated with narrow HFQPOs near 276 Hz. Type B LFQPOs (5–7 Hz, narrow profiles, lag in hard X-rays) correspond to broader HFQPOs near 184 Hz. The common type C LFQPOs (variable frequencies, narrow profiles, strong amplitude and harmonics, and small phase lags) coincide on rare occasions with HFQPOs at lower frequencies (100−169 Hz).

There are now five black hole candidates that exhibit transient HFQPOs, and for three of them there is evidence that two HFQPOs can occur simultaneously. HFQPO pairs have been seen in GRO J1655−40 (300, 450 Hz; Strohmayer 2001a; Remillard et al. 1999b), GRS 1915+105 (40, 67 Hz; Strohmayer 2001b), and also probably during the 2000 outburst of XTE J1550−564 (Miller et al. 2001). In the first two cases, Strohmayer (2001a, 2001b) investigated combinations of the azimuthal and radial coordinate frequencies in GR to explain the pair of HFQPOs, noting that other explanations are possible. For the case of GRO J1655−40, it was further claimed (Strohmayer 2001a) that the 450 Hz QPO suggests that the black hole must have substantial spin (i.e., dimensionless spin parameter $a_* > 0.15$). This conclusion uses the optically determined mass of the black hole (Shahbaz et al. 1999; Greene, Bailyn, & Orosz 2001), along with the assumption that the orbital rotation frequency (in GR) at the innermost stable circular orbit around the black hole (Shapiro & Teukolsky 1983) is the highest frequency that can be seen in the X-ray emission.

An alternative interpretation for pairs of HFQPOs utilizes "diskoseismology," which considers adiabatic perturbations in a relativistic accretion disk (Wagoner 1999; Kato 2001). If the HFQPOs in GRO J1655−40 and GRS 1915+105 represent fundamental g-mode and c-mode diskoseismic oscillations, then substantially higher values of the spin parameter are derived ($a_* \sim 0.9$ and $\sim$0.7, respectively; Wagoner, Silbergleit, & Ortega-Rodriguez 2001). For the case of GRO J1655−40, yet another interpretation was offered by Abramowicz & Kluzniak (2001), who hypothesize that there is enhanced X-ray emission at the radius in the accretion disk where there is a resonance between the Keplerian and radial coordinate frequencies. This idea is motivated by the 3 : 2 integral ratio seen in the frequencies of HFQPOs from that source. When considering all of the HFQPO observations, it is possible that the results may require more than one physical model.

As a follow-up to RSMM02, we address four questions related to QPO behavior in XTE J1550−564. (1) If we average the power density spectra (PDS) during the 1998–1999 outburst for groups defined by the LFQPO type, is there any evidence for a pair of HFQPOs? (2) Can we confirm the suggestion of Miller et al. (2001) that HFQPOs near 180 and 270 Hz occur simultaneously during the outburst of 2000? (3) Are the pairs of HFQPOs in XTE J1550−564 and GRO J1655−40 related precisely by a 3 : 2 ratio? (4) Are there X-ray spectral properties that distinguish the observations when the upper or lower HFQPO is stronger in each of these two sources?

2. OBSERVATIONS AND DATA ANALYSIS

We continue the analysis of XTE J1550−564 using *RXTE* observations reported in previous publications. For the 209 observations of the 1998–1999 outburst, spectral parameters were tabulated by Sobczak et al. (2000b). QPO properties are given in RSMM02. Timing results for 19 observations (XTE program P50134) during the outburst of 2000 April–May are reported by Miller et al. (2001). We supplement these with analyses of contemporaneous exposures under *RXTE* programs P50135 (37 observations) and P50137 (11 observations), which are now publicly available. Thus all 276 *RXTE* observations of this transient prior to the 2001 outburst are considered here.

We elaborate on our methods for conducting error analysis for features in the PDS, since the significance of QPOs is an important topic in § 3. As noted in RSMM02, the PDS (P_ν vs. ν) are computed for 256 s data segments and then averaged for each observation. We first compute the PDS using the normalization of Leahy et al. (1983) . For each frequency bin in the discrete Fourier transform ($\Delta\nu = 2^{-8}$ Hz), we compute the uncertainty as the larger of either the statistical error ($2/N^{0.5}$) or the observed standard deviation of the mean power, where there are N data segments within the observation. We then subtract the Poisson-corrected dead time, as described in Morgan, Remillard, & Greiner (1997), using the average count rates (per PCU) for good events and for very large events (which have a longer dead time) during a given observation. The PDS are then renormalized by the mean source count rate (i.e., above the nonsource background), so that the final PDS has units of (rms deviation/mean)^2 Hz^{-1}. We logarithmically rebin the frequencies using intervals that are successively larger by a factor of 1.04, propagating the uncertainty within each frequency interval. When we average the PDS for groups of observations, we compute the weighted mean (using σ^{-2}) and its uncertainty for each frequency bin.

The PDS are searched for LFQPOs (0.5–30 Hz) and HFQPOs (30–1000 Hz) separately. The search for HFQPOs uses a sliding frequency window, which typically spans $0.2\nu_{\rm trial}$ to $5.0\nu_{\rm trial}$. Within this window, the power continuum ($P_{\rm cont}$) is modeled with a second-order polynomial in $\log P_\nu$ versus $\log \nu$, since the local power continuum usually resembles a power-law function with a slight amount of broad curvature. The QPO profiles are presumed to be Lorentzian functions, and they are generally distinguished from broad peaks in the power continuum by a coherence parameter, $Q = \nu/{\rm FWHM} \gtrsim 2$. We use χ^2 minimization to obtain the best fit for the QPO profile and the local power continuum.

If the value of χ^2_ν is acceptable, and if the value with a QPO feature (i.e., six fit parameters) is less than the χ^2_ν value for a model with only the power continuum (three fit parameters), then we evaluate the significance of the QPO feature with a conservative and empirical approach, as follows. Within the central frequency range of the QPO, $\nu_0 \pm \mathrm{FWHM}$, we integrate $P_\nu - P_{\mathrm{cont}}$ and then divide the result (S) by its statistical uncertainty (σ_S), where the calculation of σ_S considers, in quadrature, the uncertainties in the power density measurements as well as the continuum fit. The uncertainty in the power continuum (at the QPO frequency) is estimated with the standard method that utilizes the second partial derivative in the surface profile of χ^2 values. Usually, σ_S is dominated by the measurement uncertainty in the power density bins, since there are many bins that constrain the continuum fit.

In the general search for HFQPOs, one should apply a significance threshold of $S/\sigma_S \gtrsim 4$, in order to report features with a high level of confidence. This compensates for the $\sim$200 trial fits computed for a given power spectrum, which is liberally estimated as the number of 2% frequency steps between 30 and 1000 Hz, where 2% is the typical uncertainty, in hindsight, for the central frequencies of broad HFQPO features. With a 4 σ threshold for HFQPO searches, we may then expect no more than one spurious HFQPO detection per 80 PDS obtained with *RXTE*.

When QPO detections are significant, we use the best-fit values for the Lorentzian peak and FWHM to compute the total integrated power (P) in the PDS feature, and the rms amplitude of the QPO is then $a = P^{0.5}$. We can then use the QPO significance as a measure of the uncertainty in P, leading to an estimate of the amplitude uncertainty, $\sigma_a/a = 0.5\sigma_S/S$. We note that the factor of 0.5 was inadvertently neglected in reporting σ_a values (overly large) in Table 1 of Remillard et al. (1999a) . Finally, we again use the second partial derivative in the surface profile of χ^2 values to estimate the uncertainties in the QPO central frequency and the QPO FWHM.

In some cases there are clear motivations to consider features at significance lower than 4 σ. For example, when a group of observations yields a highly significant HFQPO, then it is useful to analyze the individual PDS in the group near the same frequency value, e.g., with a threshold reduced to 3 σ. This type of investigation context effectively reduces the number of relevant trial fits (see Remillard et al. 1999b). An analogous topic is the detectability of any features that may be located at the harmonic frequencies related to a strong QPO detection. Below we will discuss results for such HFQPO harmonics with significances in the range 3–4 σ.

Finally, we note that global PDS modeling has been performed successfully for sources in hard X-ray states using multiple Lorentzians (Nowak 2000; Belloni, Psaltis, & van der Klis 2002; Pottschmidt et al. 2002). The results yield broad profiles ($Q < 0.5$), which distinguish these features as broad power peaks rather than QPOs. We note, however, that the multiple-Lorentzian model generally does not work well for PDS associated with the "high" or "very high" states where the power continuum roughly resembles a power-law function over several decades in frequency. This is the case for most of the observations of XTE J1550−564 that exhibit HFQPOs, and therefore a more localized fit for the power continuum is a practical necessity.

3. RESULTS

We show the results for investigations of the four questions raised in § 1. All of the power density spectra are displayed in units of $\log(\nu \times P_\nu)$ versus $\log(\nu)$, thereby making it easier to see peaks in the power density and to evaluate the relative strengths of features at widely different frequencies (Psaltis, Belloni, & van der Klis 1999; Nowak 2000). We note, however, that all of the QPO fits are computed in the (P_ν, ν)-plane.

3.1. *PDS of XTE J1550−564 during 1998–1999, Averaged by LFQPO Type*

Using Table 1 of RSMM02, we computed the average power spectra of XTE J1550−564 (6–30 keV) for groups of observations that show LFQPO types A (10 cases), B (9 cases), and C (44 of 46 cases that have data in this energy band). Observations classified A were included in the A group, but the five C cases that followed the 7.7 crab flare were not included in the C group. The results are shown in Figure 1. We have utilized the energy range 6–30 keV for this analysis, because this energy range optimizes the detections of the various HFQPOs seen in XTE J1550−564. Analogous investigations at 2–30 or 13–30 keV produce similar conclusions with weaker statistics. In RSMM02, the the broad type A LFQPOs (5–10 Hz with phase lags in soft X-rays) were associated with a narrow HFQPO near 280 Hz. In Figure 1 this HFQPO is the strongest feature in the average PDS (*top left-hand panel*), while there is also evidence of a weak feature near 185 Hz, which is not detected during any individual observation.

The narrow type B LFQPOs (5–7 Hz, strong harmonics, hard lags) are associated with a broader HFQPO near 185 Hz. In Figure 1 (*bottom left*), the average B-type PDS clearly shows the LFQPO, its harmonics at $0.5\nu_0$ and $2\nu_0$, and the strong peak at 185 Hz. There is also complex structure and possibly additional HFQPOs on both sides of the 185 Hz feature. Type C LFQPOs (ν_0 varying from 0.08 to 7 Hz, weak phase lags) are smeared out in the average C-type PDS (Fig. 1, *top right-hand panel*), which is dominated by a continuum that may be deconvolved into three or more broad power peaks. For the C-type PDS, the integrated rms fractional variability (0.1–1000 Hz) is 0.21 at 6–30 keV, while the total power for types A and B is only 0.04–0.08 at 6–30 keV. Finally, the bottom right-hand panel of Figure 1 shows the PDS for 1998 September 19, when XTE J1550−564 was in the midst of a flare to a peak intensity of 7 crab (see e.g., Sobczak et al. 2000b). Significant QPOs are seen at 4.9, 13.2, and 183 Hz on that occasion.

To quantify the significance of the weaker, high-frequency features in the PDS of types A and B, we modeled the data in the range 20–2000 Hz according to the procedures described in § 2. In each of these fits, the central frequencies are forced to have ratios of 2 : 3 or 1 : 2 : 3, and their positions are adjusted with one free parameter. The results are shown in Figure 2. The top two panels show QPO fits for the type A and type B groups; the PDS data are the same as those plotted in Figure 1. The best-fit models for the QPO profiles are shown with dark lines, the power continuum is shown with a dashed line, and the central QPO frequencies in the model are shown with vertical ticks above the data. We note that our dead-time correction model chronically leaves residual power at the level of $P_\nu \sim 10^{-6}$ Hz^{-1} (see

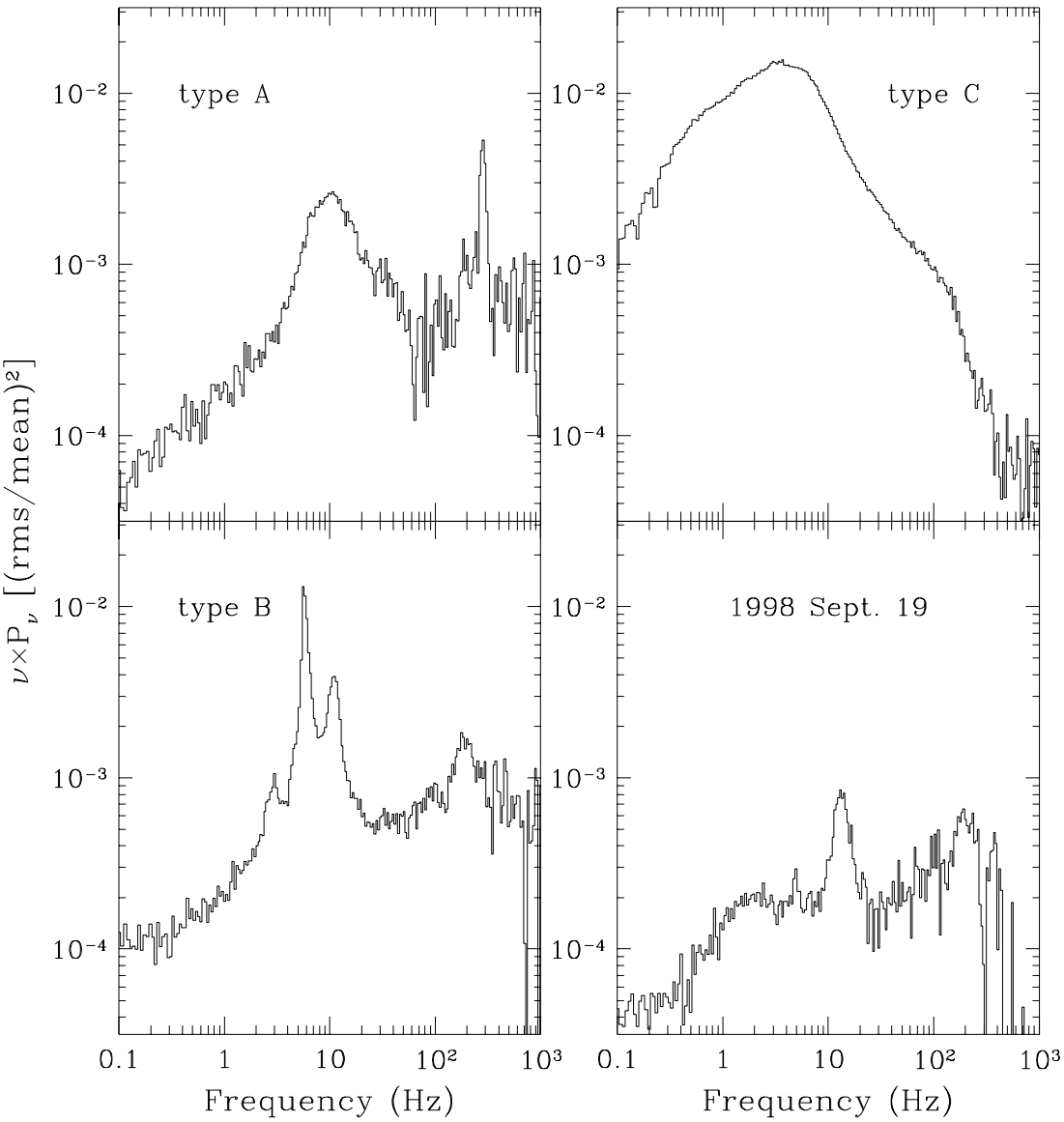

FIG. 1.—Average power spectra for observations of XTE J1550−564 grouped by the type (A, B, or C) of low-frequency QPOs that were observed during the 1998–1999 outburst. We also show the PDS for the intense 7 crab flare that was sampled on 1998 September 19.

Revnivtsev, Gilfanov, & Churazov 2000 for further discussions of this effect). Thus, with the PDS displayed in $\log(\nu \times P_\nu)$ units, the power continuum (*dashed line*) shows some upward curvature while smoothly connecting the source power below 100 Hz to the residual dead-time effects at 1 kHz.

All of the QPO parameters derived from these profile models are given in Table 1. For the type_A PDS, the significance of the weaker feature at 187 Hz (Fig. 2, *top panel*) is above 4 σ. For the type B PDS, both the shallow QPO found at 92 Hz and the weak feature near 278 Hz are above 3 σ. We interpret these results as evidence that the HFQPOs near 185 and 280 Hz coexist and that there are harmonic relationships in the HFQPOs in XTE J1550−564. The type B PDS seems to exhibit the highest harmonic content. We note the hints of weak features seen at the fourth and fifth harmonics (each near 2 σ), as shown with arrows in Figure 2 (*middle panel*). We further acknowledge the need to confirm these results, for this source and for other black hole binaries as well. This is particularly important for the QPO at the fundamental frequency (92 Hz), since the detection has only modest significance and since broad QPO features are susceptible to systematic uncertainties related to the method to model the power continuum.

3.2. *HFQPOs in XTE J1550−564 during the Outburst of 2000*

We also examine data from the second outburst of XTE J1550−564, which began around 2000 April 4. Miller et al. (2001) reported six detections of a QPO near 270 Hz out of a total of 12 *RXTE* observations that were made between 2000 April 30 and May 9. This time interval occurs just after the time of maximum luminosity (April 29), as seen with the *RXTE* All-Sky Monitor. In the average PDS for these six observations, QPOs were found at 268 ± 3 Hz (7.8 σ) and 188 ± 3 Hz (3.5 σ), suggesting that the features appear simultaneously (Miller et al. 2001).

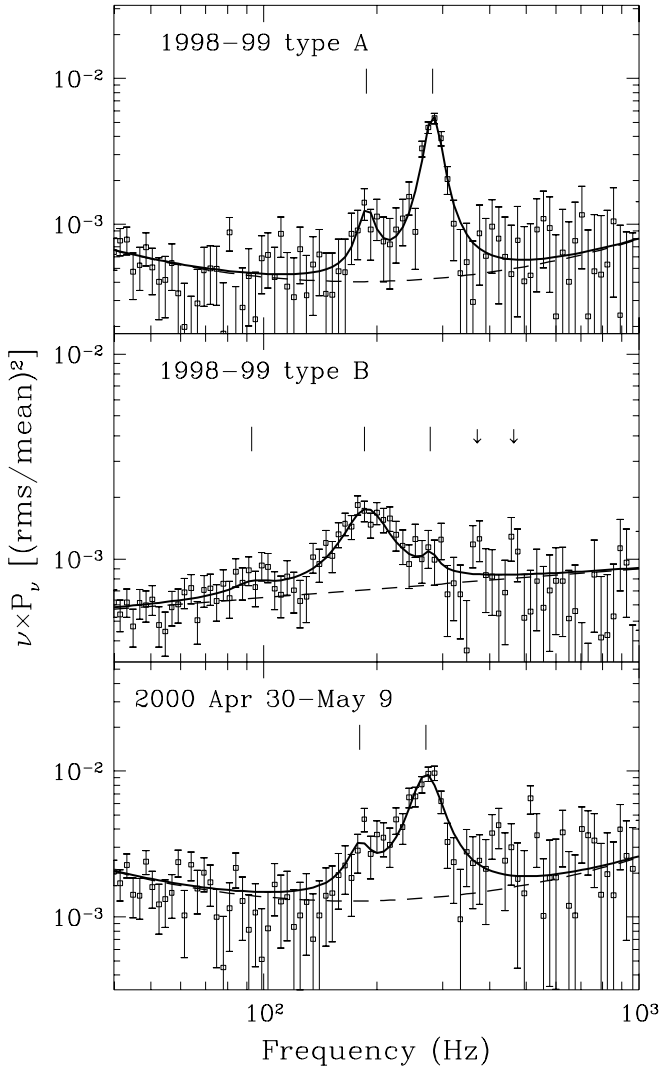

FIG. 2.—Fits for harmonically related HFQPOs in XTE J1550−564 in power spectra at 6−30 keV. The top two panels show the same data displayed in Fig. 1. The bottom panel shows the QPO fit for the average of 12 observations between 2000 April 30 and May 9. In each panel the tick marks above the data show the central frequencies of significant QPOs. The best fit is shown with a smooth, dark curve, and the power continuum is shown with a dashed line. For the type B group (*middle panel*), the arrows show the expected locations of the fourth and fifth harmonics.

Here we add two details to the findings of Miller et al. (2001), who reported strong HFQPO detections by selecting PCA data above 6 keV. First, we find one additional HFQPO detection at 267 ± 8 Hz ($Q = 4.9$) on 2000 May 5. The significance is highest (4.5 σ) for data in the energy range 2–30 keV. Second, for the five remaining observations during 2000 April 30–May 9, we find that their average PDS contains a significant QPO near 270 Hz. We therefore combine all 12 observations (6–30 keV) to further test the significance of a second QPO near 180 Hz and to help judge the acceptability of a model with forced harmonic relationships in the central frequencies. The results (Fig. 2 and Table 1) support the conclusion by Miller et al. that the pair of QPOs occur simultaneously, and the significance of the second QPO near 180 Hz is increased to 5 σ by averaging together all 12 observations.

The central frequencies (independently fitted) derived by Miller et al. (2001) deviate from a ratio of 3 : 2 by 2.2 σ. For the 12 observations in the same time interval (Fig. 2, *bottom*), the harmonic fit is acceptable. Comparing the QPO profile model with the data, one can see that the peak at lower frequency might move to slightly higher frequency if it were treated as a free parameter. Since the six QPO detections (Miller et al. 2001) decrease in central frequency with time (276–249 Hz), small deviations from a 3 : 2 frequency ratio could arise from changes in the relative strength of the two features during the sampling interval. We conclude that the QPO properties during the 2000 outburst of XTE J1550−564 are amenable to interpretation via a harmonic relationship, but alternative possibilities cannot be excluded.

3.3. *Summary of HFQPOs in XTE J1550−564*

There are now 28 HFQPO detections reported for individual observations of XTE J1550−564 (Homan et al. 2001; RSMM02; Miller et al. 2001; Kalemci et al. 2001; § 3.2). Their central frequencies vary substantially, but the majority tend to cluster near 184 or 276 Hz. This is evident in the histogram of HFQPO frequencies shown in Figure 3 (*top*). In making the histogram, we varied the binning intervals to maintain a width of ±5% relative to the central frequency.

None of the individual observations yield detections of a pair of HFQPOs, yet when groups of observations are averaged, either by the LFQPO type (1998–1999) or by time interval (2000), we find three HFQPOs organized as harmonics near 92, 184, and 276 Hz. These results suggest that the HFQPO harmonics appear simultaneously but that only the dominant feature is detectable in the individual observations.

We next assess the extent to which any individual HFQPO detections occur well outside of this harmonic scheme. In most cases (17 of 28), the allowed range of frequencies ($\nu \pm 1$ σ) lies within 3% of a harmonic value. At the other extreme, three of 28 cases deviate from a harmonic value by an amount greater than 12%. One of these is the 65 Hz QPO reported by Kalemci et al. (2001) for 2000 May 20. We find the significance of this feature to be below 4 σ. The two others were observed on 1998 October 15 (with type C LFQPOs), and their average PDS is shown in Figure 4. The QPO (5.0 σ) is found at 143 ± 8 Hz, which is closer to the geometric mean of the harmonics than it is to either 92 or 184 Hz. Even though the statistical quality of the data is limited, it is important to note that the harmonic scheme may represent only a subset of the behavior patterns of HFQPOs in XTE J1550−564. One final note concerns the narrow QPO reported at 123 Hz for 1999 May 17 by Homan et al. (2001). In our analysis of the same observation (RSMM02), we find a broader QPO at 209 Hz, and so we do not see this case as a clear challenge to the interpretation of harmonic HFQPO frequencies.

3.4. *X-Ray Spectra and HFQPOs in XTE J1550−564*

We now focus attention on the spectral properties that may distinguish which harmonic frequency is present in each observation that exhibits an HFQPO. XTE J1550−564 displays a typical X-ray spectrum for a black hole binary, with a thermal component from the accretion disk and a hard power-law attributed to inverse Compton scattering by electrons of unknown origin. Sobczak et al. (2000b) deconvolved these spectral components and reported

TABLE 1
QPO Fit Parameters[a]

Parameter	1998–99 A	1998–99 B	1998 Sep 19	2000 Apr 30–May 9
Number of objects	10	9	1	12
Source intensity (crab units)	0.3–2.0	1.3–1.8	6.5	0.3–1.0
χ^2_ν	0.67	0.82	1.11	0.86
QPO near 276 Hz				
Frequency (Hz)	281.7 (1.5)	277.7	...	269.4 (2.7)
Significance (σ)	16.8	3.5	...	14.4
FWHM	33.7 (2.4)	27.9 (15.6)	...	57.7 (4.9)
Q (ν/FWHM)	8.4 (0.6)	10.0 (5.6)	...	4.7 (0.4)
Amplitude	3.13 (0.09)	0.55 (0.08)	...	5.24 (0.18)
QPO near 184 Hz				
Frequency (Hz)	187.8	185.1 (3.5)	187.4 (5.6)	179.6
Significance (σ)	3.9	12.5	10.4	5.2
FWHM (Hz)	22.7 (9.1)	62.3 (6.2)	87.1 (11.1)	29.5 (12.2)
Q (ν/FWHM)	8.3 (3.3)	3.0 (0.3)	2.2 (0.3)	6.1 (2.5)
Amplitude (rms %)	1.20 (0.15)	2.34 (0.09)	1.72 (0.08)	1.95 (0.19)
QPO near 92 Hz				
Frequency (Hz)	...	92.6	...	...
Significance (σ)	...	3.2	...	...
FWHM (Hz)	...	27.0 (17.8)	...	...
Q (ν/FWHM)	...	3.4 (2.2)	...	...
Amplitude (rms %)	...	0.64 (0.10)	...	...

[a] Uncertainty estimates (1 σ confidence) are given in parentheses. Since the model includes only one free parameter for frequency, the uncertainty in the frequency is listed for the harmonic that dominates the fit. All of the QPO results pertain to the spectral range 6–30 keV, while the source intensity is evaluated at 2–10 keV, where 1 crab $= 2.4 \times 10^{-8}$ ergs cm^{-2} s^{-1}.

parameters for the 209 *RXTE* observations obtained during the 1998–1999 outburst. We performed the same analysis for the 43 *RXTE* observations obtained during 2000 in order to compare the behavior of the source during the two outbursts.

It has been shown that the exercise of plotting the integrated disk flux versus power-law flux in black hole binaries is very useful in tracking the flow of energy between the two components through different X-ray states and also in relating QPO parameters to spectral parameters (Muno, Morgan, & Remillard 1999; Sobczak et al. 2000a). Using the spectral parameters of Sobczak et al. (2000b), we show the flux measures in the two spectral components during the 1998–1999 outburst in Figure 5. As discussed in RSMM02, one can integrate the spectral components either over the PCA energy range with highest sensitivity (2–25 keV) or over bolometric limits, in which case the majority of the disk flux is extrapolated below 2 keV. Both options are displayed in Figure 5. For the bolometric estimates, the lower limit on the integration of the power-law component is reduced to 1 keV, which affects the results significantly when the power-law spectrum is steep. The typical flux uncertainties (see Table 3 of Sobczak et al. 2000b) are in the range $(0.2–0.3) \times 10^{-8}$ ergs cm^{-2} s^{-1}, which is smaller than the symbol size in Figure 5.

We note that the bolometric disk flux is $2.16 \times 10^{-11} N_{\rm dbb} T^4$ ergs cm^{-2} s^{-1}, where $N_{\rm dbb}$ is the multitemperature disk normalization: $N_{\rm dbb} = R_{\rm in} \cos\theta / d^2$, with the inner disk radius, $R_{\rm in}$, expressed in kilometers and the distance, d, in units of 10 kpc. Assuming a disk inclination $\theta = 72°$ and $d = 6$ kpc (Orosz et al. 2002), then the bolometric disk luminosity would be 1.3×10^{39} ergs s^{-1} (or 1.0 $L_{\rm Edd}$ for a 10 $M_\odot$ black hole) for a value of 17.9×10^{-8} ergs cm^{-2} s^{-1} in the left-hand panel (*horizontal axis*) in Figure 5. For the power-law component, the luminosity depends only on d, and the corresponding value (*vertical axis*) is 29.2×10^{-8} ergs cm^{-2} s^{-1}.

In Figure 5 we use the symbol color to denote the following QPO conditions: HFQPO detections (*blue*), LFQPOs only (*green triangle*), and no QPOs (*red cross*). In addition, the shape of the blue symbols distinguishes the HFQPOs near 92 Hz (*open square*), 184 Hz (*filled square*), and 276 Hz (*star*). The results for the pair of observations on 1998 October 15 (anomalous 143 Hz QPO) are displayed with blue circles. There are clear patterns in these results, and the conclusions do not depend on the integration limits used to calculate the flux (compare the left- and right-hand panels). There is a fairly well-defined horizontal branch (*red crosses*) in which the disk dominates the spectrum and no QPOs are seen, just as in the case of GRS 1915+105 (Muno et al. 1999). The large majority of vertical excursions from this branch display some kind of QPO activity. These spectra with enhanced power-law flux occur over a wide range of disk flux. Similar effects are seen in the color-color diagrams of XTE J1550−564 (Homan et al. 2001). The complexity of these "hard branches" contrasts with the relative simplicity of the vertical branch (radio-loud) at very low disk flux in the case of GRS 1915+105 (Muno et al. 1999) and also the branch for hard flares in GRO J1655−40, which is shown below.

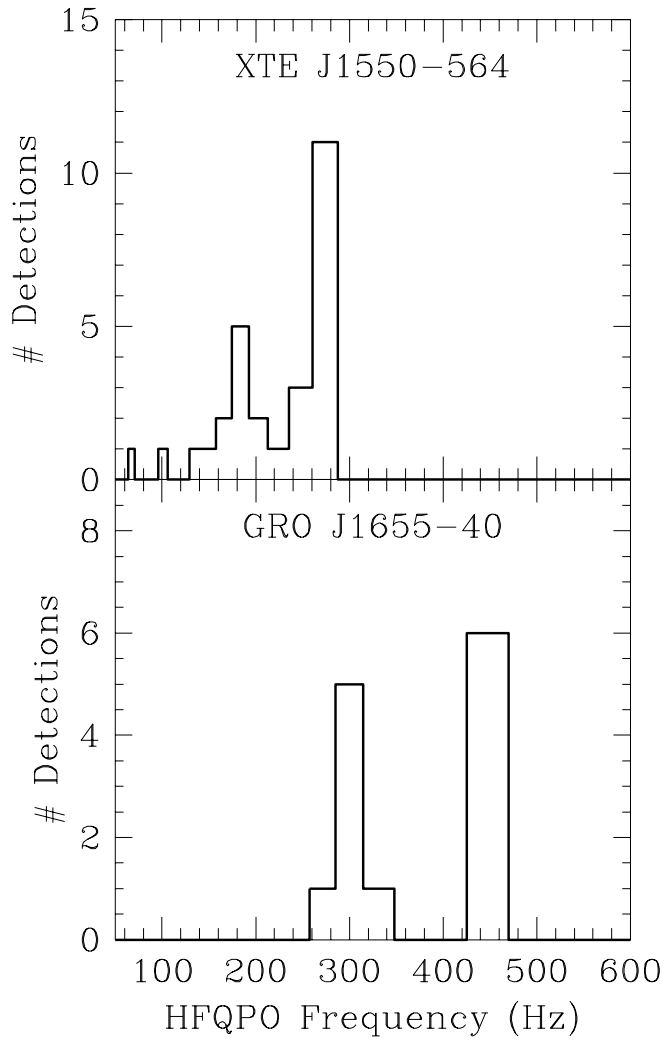

FIG. 3.—Histogram of HFQPO frequencies for XTE J1550−564 and GRO J1655−40. The binning intervals are varied to maintain a width of ±5% relative to the central frequency. Each source displays two peaks in the distribution that have a 3 : 2 ratio in frequency.

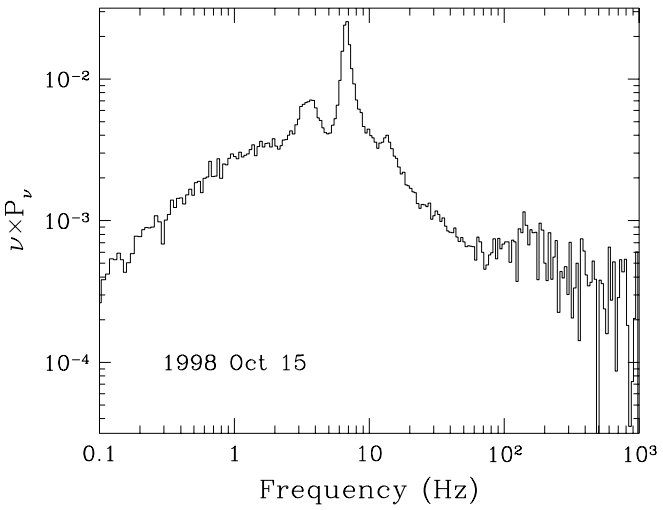

FIG. 4.—Average power spectrum for XTE J1550−564 for the two observations made on 1998 October 15. The QPO at 143 ± 8 Hz represents the most significant deviation from the harmonic scheme (92, 184, 276 Hz) that accounts for most of the HFQPO detections in this source.

The spectral diagrams in Figure 5 also distinguish the HFQPOs and the selection of different harmonic frequencies at different times. There is a systematic difference in magnitude of the power-law flux between the points associated with the 276 Hz QPO (*blue stars*) versus the 184 Hz QPO (*filled blue squares*). The X-ray spectra associated with the 276 Hz QPO lie systematically closer to the horizontal branch in which the spectrum is dominated by the accretion disk.

We present the same diagrams for the much weaker outburst of 2000 in Figure 6. This outburst samples different X-ray states and reaches a maximum luminosity that is a factor of 10 below the levels seen during 1998–1999. Here all of the HFQPO detections associated with the 276 Hz feature (*blue stars*) occur at approximately the same disk and power-law fluxes as their counterparts in Figure 5, and they again lie close to the disk-dominant branch (*red crosses*) plotted in Figure 5. The observations during the time interval of 2000 April 30–May 9 correspond to the 12 red and blue points in the lower right-hand quadrant of the right panel in Figure 6. We have shown that the average PDS for these observations exhibits a strong QPO at 270 Hz accompanied by a 5 σ detection at 180 Hz (Fig. 2 and Table 1). We conclude that these spectral and specific temporal results for the 2000 outburst support the idea that HFQPOs near 184 and 276 Hz represent a temporal signature of accretion that is inherent to this black hole binary system.

Finally, we note that XTE J1550−564 additionally displays a vertical branch (*green triangles*) during the 2000 outburst (Fig. 6) in which the power-law component varies while there is little contribution from the disk. At these times the PDS show only LFQPOs and strong continuum power. These observations are further associated with a steady jet seen in the radio band (Corbel et al. 2001). A similar X-ray track associated with a flat radio spectrum has been seen in GRS 1915+105 (Muno et al. 1999).

3.5. *Summary of HFQPOs in GRO J1655−40*

HFQPOs near 300 Hz at photon energies of 2–30 keV were reported for six observations of GRO J1655−40 by Remillard et al. (1999b), (significance $\gtrsim 3\ \sigma$). We examined *RXTE* pointings under programs 10261 and 20187 (which were not available for that paper) and report an additional strong detection (6.0 σ) at 320 ± 11 Hz (with $Q = 4.6$) for the observation on 1996 November 7. There is no detection of a QPO near 450 Hz in this observation.

Strohmayer (2001a) reported detections of five HFQPOs near 450 Hz for PDS computed using data from photon energies in the range 13–27 keV. Again, the analysis of the data from these other programs yields an additional, weak detection (3.4 σ at 13–27 keV) at 447 ± 5 Hz (with $Q = 8.9$) for the observation on 1996 June 20. There is no 300 Hz QPO detection during that observation.

These results raise the total to 10 observations in which one or more HFQPOs are detected in GRO J1655−40: four show only the 300 Hz QPO, three show only the 450 Hz QPO, and three show both. For the three observations that exhibit both HFQPOs (Strohmayer 2001a), the independent profile fits (using different energy bands) yield central frequencies of 295 ± 4 Hz (2–30 keV) and 440 ± 5 Hz (13–30 keV), respectively. These results are consistent with a 3 : 2

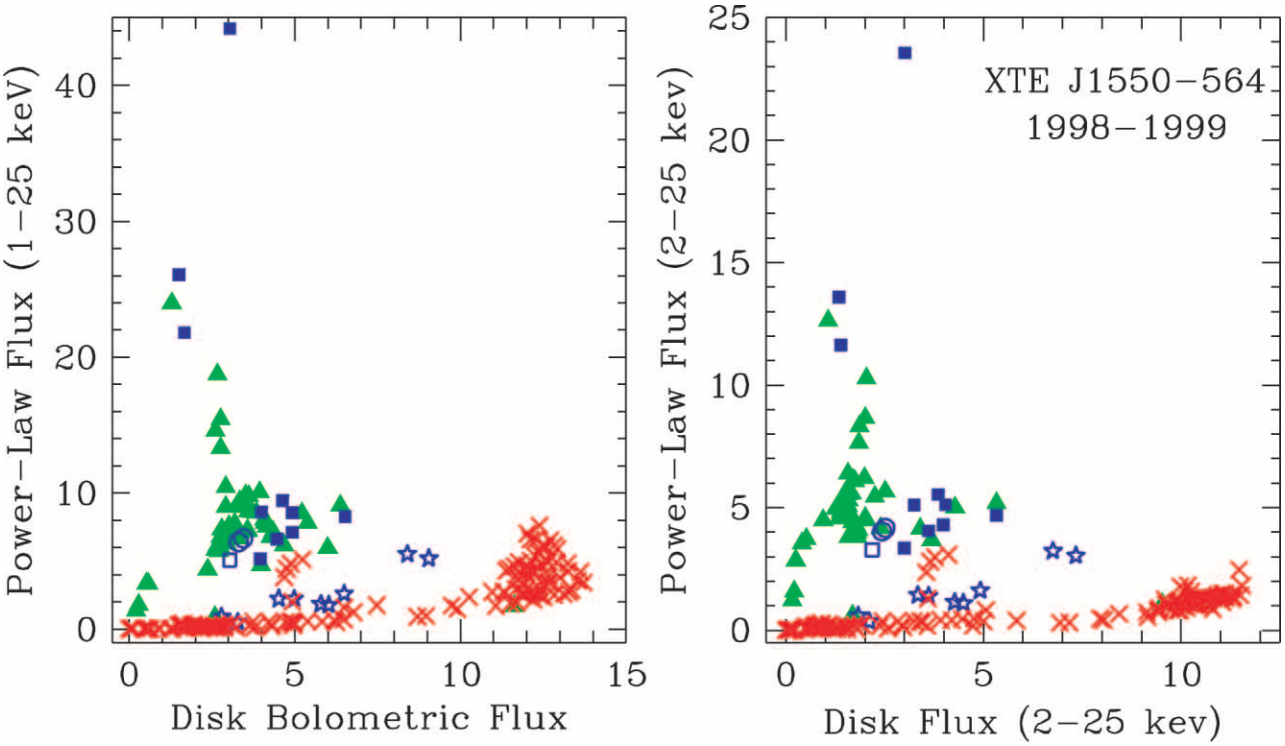

FIG. 5.—Energy spectrum decomposition for XTE J1550−564 during the 1998–1999 outburst. The flux units are 10^{-8} ergs cm^{-2} s^{-1}, and the statistical uncertainties are smaller than the symbol size. The flux from the accretion disk and the X-ray power law are shown in conventions of both bolometric flux (extrapolated; *left*) and apparent flux (2–25 keV; *right*). The color and type of plotting symbol denotes the QPO condition: HFQPO detection (*blue*), only LFQPO (*green triangle*), and no QPO (*red cross*). In addition, the shape of the blue symbol distinguishes an HFQPO near 92 Hz (*open square*), 184 Hz (*filled square*), and 276 Hz (*star*). The two observations of 1998 October 15 are shown with blue circles. In either flux convention (bolometric or apparent), there is a systematic shift away from disk-dominated track (*red crosses*) as the detected HFQPO shifts from 276 to 184 Hz.

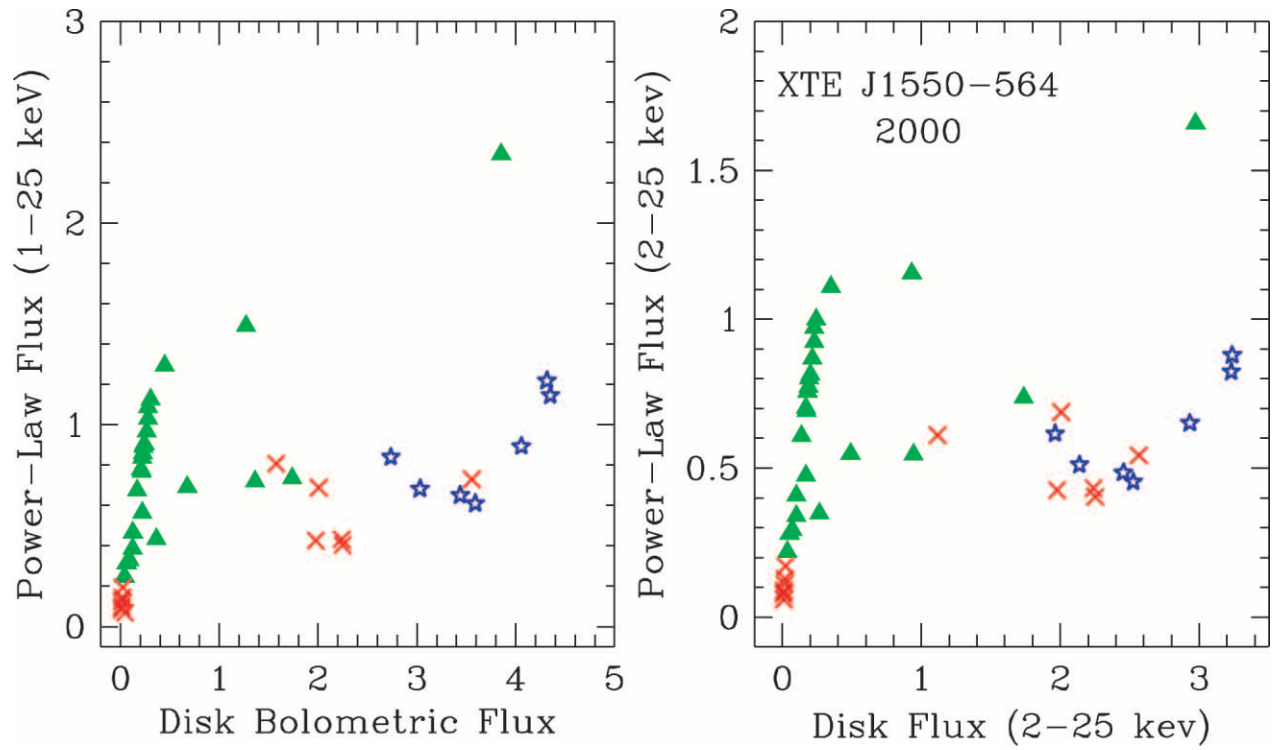

FIG. 6.—Energy spectrum decomposition for XTE J1550−564 during the outburst of 2000. The flux units and symbol types follow the definitions given for Fig. 5. In this outburst there is a track in which the power-law spectrum dominates (*green triangles*), and the points associated with HFQPOs near 276 Hz (*blue stars*) are again close to the disk-dominated track shown in Fig. 5.

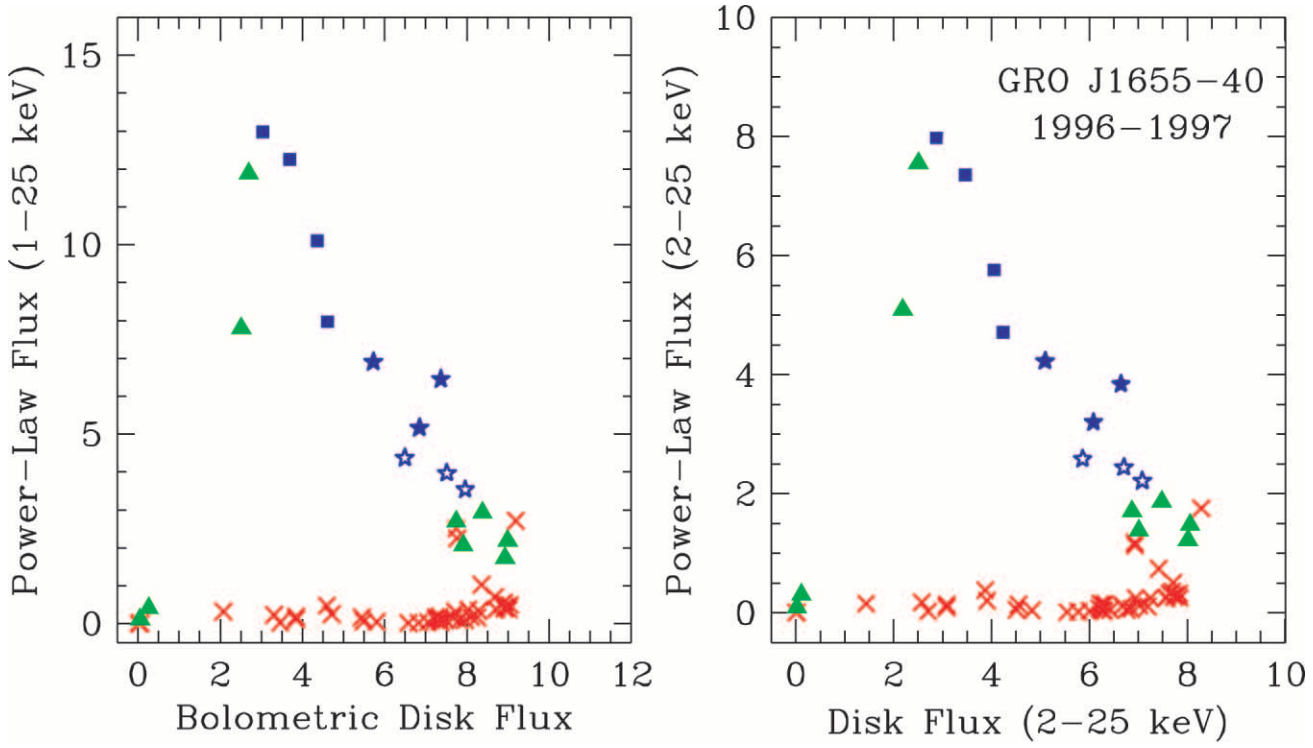

FIG. 7.—Energy spectrum decomposition for GRO J1655−40 during its outburst of 1996–1997. The flux units and symbol types follow the definitions given for Fig. 5, except that the HFQPO symbols refer to the 300 Hz QPO (*filled blue square*) and 450 Hz QPO (*open blue star*), respectively. In addition, the observations that exhibit both 300 and 450 Hz QPOs are shown with a filled blue star. The results are very similar to those for XTE J1550−564 (Fig. 5). There is increasing power-law flux as the strongest HFQPO shifts from the 450 Hz feature (*open blue stars*) to the 300 Hz feature (*filled blue squares*).

ratio, as noted in § 1, while one feature is usually much stronger than the other, as seen in the behavior of XTE J1550−564. In the next section, we examine whether the X-ray spectra evolve in parallel with the relative strength of the HFQPO features in the case of GRO J1655−40.

3.6. *X-Ray Spectra and HFQPOs in GRO J1655−40*

We use the 52 spectral observations reported by Sobczak et al. (1999), supplemented by similar analyses for *RXTE* programs 10261 (six spectra binned in 1 day intervals), 20187 (1996 November 7), and 20402 (the final three observations, not reported previously). In addition, since there is so much exposure time during 1996 May 9–11, we choose to sample the data in seven time intervals, rather than in three daily bins. This yields a net of 66 spectral observations of GRO J1655−40. We display the results of the spectral decomposition in Figure 7. The procedures are the same as those conducted for XTE J1550−564, except that we use an inclination angle of 70° and a distance of 3.2 kpc for GRO J1655−40 (Greene, Bailyn, & Orosz 2001 and references therein). In this case, the disk luminosity would be 7.9×10^{38} ergs s^{-1} (or 1.0 $L_{\rm Edd}$ for a 6.3 $M_{\odot}$ black hole) for a bolometric disk flux of 45×10^{-8} ergs cm^{-2} s^{-1} in the left-hand panel (*horizontal axis*) of Figure 7. For the power-law component, the same luminosity corresponds to 65×10^{-8} ergs cm^{-2} s^{-1} in the same figure panel (*vertical axis*). The spectral analyses (Sobczak et al. 1999) yielded typical flux uncertainties in the range $0.1–0.2 \times 10^{-8}$ ergs cm^{-2} s^{-1}. Therefore, in Figure 7 the errors are again smaller than the symbol size.

For GRO J1655−40, the relationship between HFQPO properties and the energy division between the spectral components resembles the results for XTE J1550−564 in several important ways. The observations with HFQPOs (*blue symbols*) lie above the horizontal branch (*red crosses*) where the disk dominates the spectrum and no QPOs are seen. Moreover, with increasing power-law luminosity we see the following progression: first are the observations where we detect only the 450 Hz QPO (*open blue stars*), next are cases in which both HFQPOs are detected simultaneously (*filled blue stars*), finally there are those in which only the 300 Hz QPO is seen (*filled blue squares*). This is the same pattern seen for XTE J1550−564, where the strongest modulation shifts from 276 to 184 Hz as the power-law flux increases (cf. Fig. 5). This similarity suggests that the physical process that produces HFQPOs in these two sources is identical.

4. DISCUSSION

The 3 : 2 : 1 frequency ratio with a fundamental frequency near 92 Hz seems to account for most of the X-ray HFQPOs detected in 28 individual observations of XTE J1550−564. The features seen in the average PDS for three well-defined groups of observations support this scheme and further suggest that the HFQPO harmonics may coexist. Moreover, all of the 13 HFQPO detections (in 10 observations) in GRO J1655−40 conform to a 3 : 2 frequency ratio with an implied fundamental at 150 Hz, including the three occasions in which both the 300 and 450 Hz QPOs were detected (Strohmayer 2001a). These results provide solid evidence for harmonic relationships between the HFQPOs in black hole binaries, Nevertheless we acknowledge the need to confirm this conclusion in these and other X-ray sources, since many

of the detections are near the statistical threshold for high levels of confidence.

We have found that the concurrent evolution of the HFQPOs and the X-ray spectra is very similar for these two black hole binaries. The primary result is an increase in the luminosity of the X-ray power-law component as the HFQPOs exhibit a shift from the third harmonic to the second harmonic. We also note that HFQPOs are generally not detected along the spectral tracks in which either the accretion disk or the power-law component strongly dominates the spectrum (i.e., the horizontal, red tracks in Figs. 5 and 7 and the vertical, green track in Fig. 6). The energy decomposition diagrams do not show perfect segregation of points relative to the HFQPO properties. However, we cannot expect perfect organization, given the variations in statistical sensitivity. The primary limitation is the ability to detect HFQPOs (and hence define the symbol type), since these oscillations have rms amplitudes of only 0.5%–5% of the mean count rate in the selected energy band.

The deduced fundamental frequencies for the HFQPOs in XTE J1550−564 (92 Hz) and GRO J1655−40 (150 Hz) differ by a factor of 1.63 ± 0.06. On the other hand, the inverse ratio of black hole masses is 1.59 ± 0.27 (Orosz et al. 2002; Greene et al. 2001), suggesting that the fundamental frequencies scale as M^{-1}. This result is generally consistent with the known mechanisms related to disk oscillations in the strong-field regime of general relativity, as long as the values of the spin parameter (a_*) are similar for these two black holes. These results illustrate both the quantitative value of HFQPO detections as a means of probing the physical properties of black holes, and also the need to continue efforts to independently measure black hole masses via dynamical optical studies.

If these HFQPOs are indeed harmonically related, then we must attempt to specify a physical model that accounts for the oscillation frequencies, provides an emission mechanism that produces HFQPOs (especially at the second and third harmonics), and explains the spectral evolution associated with the harmonic order. The results for XTE J1550−564 further suggest the need to accommodate occasional shifts in the frequency system (e.g., ~10% shifts occur ~15% of the time and perhaps ~30% shifts occur on rare occasions). With regard to the largest shifts, it is also possible that some HFQPOs involve a different physical mechanism, as suggested for the HFQPO pair at 40 and 67 Hz in GRS 1915+105 (Strohmayer 2001b). Finally, if the oscillations originate in the inner accretion disk, there is a need to understand why there are no HFQPOs detected when the accretion disk dominates the spectrum (Figs. 5 and 7, *red crosses*). Below we discuss two types of inner disk oscillations, while noting that we cannot exclude the possibility that high-frequency oscillations are rooted in the physics of a corona associated with the power-law component.

4.1. *Resonance in GR Coordinate Frequencies in the Inner Disk*

At the radii in the accretion disk where most of the X-rays originate, the coordinate frequencies in GR are predicted to have nonintegral ratios. The 3 : 2 frequency ratio in the HFQPOs in GRO J1655−40 was therefore seen by Abramowicz & Kluzniak (2001) as remarkable support for their idea that QPOs may result from a resonance between the orbital (i.e., azimuthal) and radial coordinate frequencies in the inner disk. Unlike the orbital and polar frequencies, the radial coordinate frequency reaches a maximum value at a radius larger than the innermost stable orbit, regardless of the values of black hole mass and spin (see Kato 2001; Merloni et al. 1999; and references therein). For a wide range in the dimensionless spin parameter, a_*, one can find a particular radius that corresponds to a 2 : 1, 3 : 1, or 3 : 2 ratio in the orbital and radial coordinate frequencies. In the resonance model, nonlinear perturbations may grow at these radii, ultimately producing X-ray oscillations that represent some combination of the individual resonance frequencies, their sum, or their difference. The proper interpretation of observed HFQPO frequencies may then constrain the black hole spin parameter, if the mass is known via dynamical studies of the binary companion. For GRO J1655−40, Abramowicz & Kluzniak (2001) constrain the spin parameter to the range $0.2 < a_* < 0.67$ for a black hole mass in the range 5.5–7.9 $M_\odot$. For the same limits in black hole mass and spin, the resonance radius occurs in the range $4.1R_g$–$7.2R_g$, where $R_g = GM/c^2$. We calculate that the resonance radius in these cases lies in-between the innermost stable orbit ($3.5R_g$–$5.3R_g$) and the radius of maximum surface emissivity ($5.4R_g$–$8.4R_g$; Merloni et al. 1999; Zhang, Cui, & Chen 1997). Resonance may therefore occur near radii already expected to yield X-ray emission.

For the case of XTE J1550−564, a black hole mass of 8.5–11.5 $M_\odot$ (Orosz et al. 2002) can be combined with the HFQPO oscillations to constrain the value of a_* using the resonance model, as shown in the top left-hand panel of Figure 8. The blue-shaded tracks show values of black hole mass and spin that produce orbital and radial coordinate frequencies that are within 2% of 184 and 92 Hz (*left track*), respectively, or 276 and 92 Hz (*right track*), respectively. There is only a tiny corner of parameter space (near $a_* = 1$) that may yield an orbital : radial resonance near 276:184 Hz. Excluding this region, the model for a resonance in the orbital and radial coordinate frequencies limits the black hole spin to $0.1 < a_* < 0.6$. At the lower spin limit (8.5 $M_\odot$ and the 2 : 1 resonance), the resonance radius is 7.5 R_g, while the innermost stable orbit is 5.6 R_g and a maximum surface emissivity (with no resonance) would occur at 8.8 R_g. At the spin upper limit (11.5 $M_\odot$ and a 3 : 1 resonance) the resonance occurs at 4.5 R_g, with a last stable orbit of 3.9 R_g and maximum surface emissivity at 6.0 R_g.

In the lower panel of Figure 8 we illustrate the same resonance tracks for GRO J1655−40, using the range 5.8–6.8 $M_\odot$ (Greene et al. 2001) and matching the orbital and radial coordinate frequencies to within 2% of 300 and 150 Hz (*left track*), respectively, or 450 and 150 Hz (*right track*), respectively. In this case, there is no combination of allowed mass, a_*, and r that produces orbital and radial frequencies at 450 and 300 Hz, respectively (i.e., a 3 : 2 resonance), as noted by Abramowicz & Kluzniak (2001) previously. For GRO J1655−40, the orbital : radial resonance model yields $0.24 < a_* < 0.58$. The results of Abramowicz & Kluzniak (2001) differ slightly because they used broader mass constraints (5.5–7.9 $M_\odot$; Shahbaz et al. 1999).

For completeness, we also consider the possibility of a resonance between the polar and radial coordinate frequencies, and the results for the two black hole systems are shown in the right-hand panels of Figure 8. A polar : radial resonance allows a broader range in the spin parameter, and the three blue-shaded tracks correspond to 2 : 1, 3 : 1, and

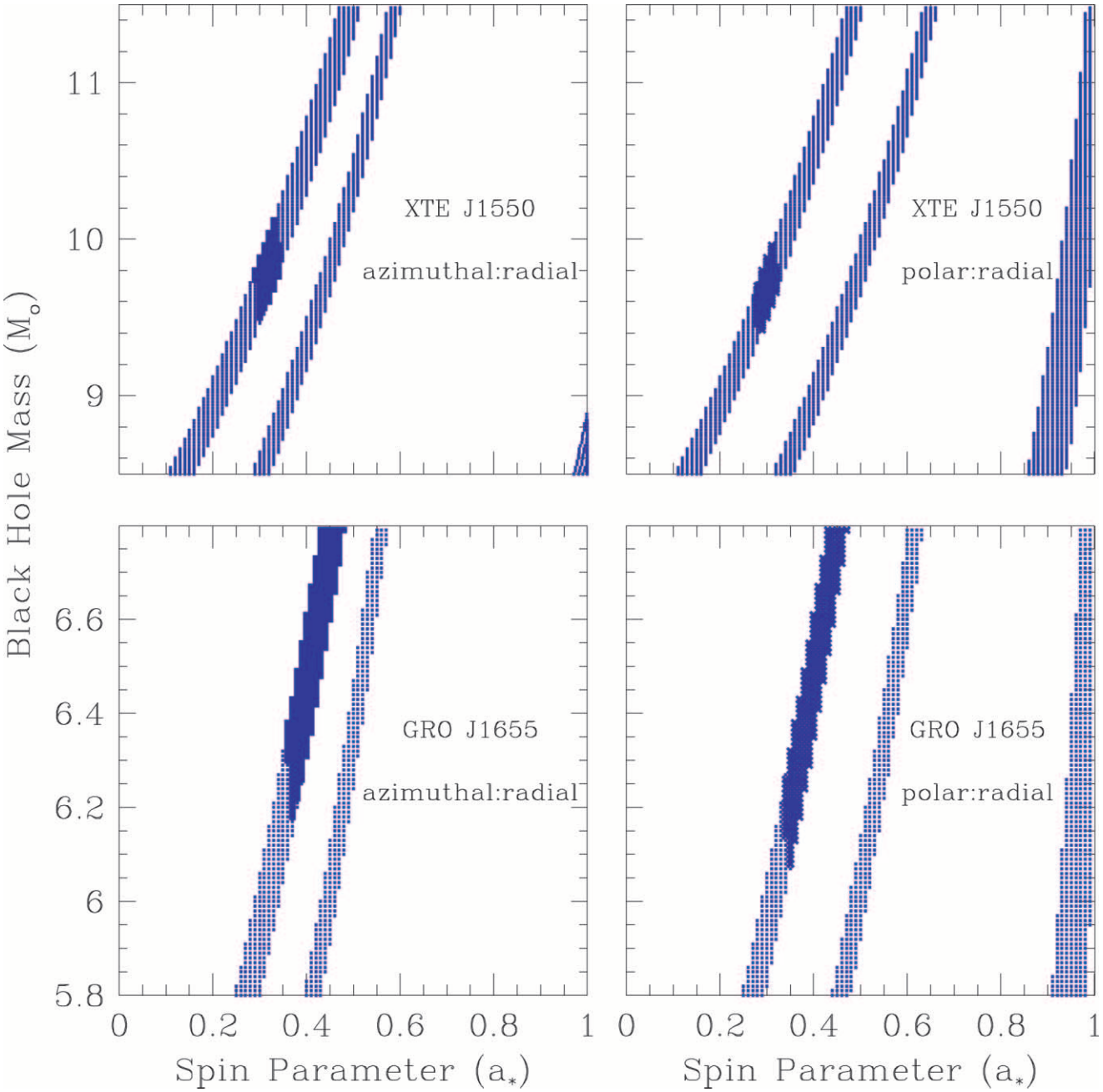

FIG. 8.—Application of the coordinate-frequency resonance model to the HFQPOs in XTE J1550−564 (*top panels*) and GRO J1655−40 (*bottom panels*). In the left-hand panels, the blue-shaded regions show mass and spin values that would allow a match (within 2%) between an azimuthal : radial resonance and the observed HFQPO frequencies. Similarly, the right-hand panels match HFQPOs and resonances between polar and radial coordinate frequencies. In each of the four panels, the leftmost track corresponds with a 2 : 1 resonance (i.e., 184 : 92 Hz in the top panels and 300 : 150 Hz in the bottom panels). The next track at higher spin corresponds with the 3 : 1 resonance (276 : 92 Hz in the top panels and 450 : 150 Hz in the bottom panels). A 3 : 2 resonance corresponds to the tracks with highest spin in the case of polar : radial resonance (*right panels*) and in the corner of the azimuthal : radial resonance for XTE J1550−564. The regions shaded with darker blue show the parameter space that additionally yields a frame-dragging frequency (at the resonance radius) that is consistent with observed LFQPOs (i.e., 5.8–6.4 Hz for XTE J1550−564 and 12.2–17.5 Hz for GR) J1655−40. We caution that the association of LFQPOs with the frame-dragging frequency is highly speculative.

3 : 2 resonances (in order of increasing a_*), respectively, matched to the HFQPO frequencies for each X-ray source.

In both X-ray sources the HFQPO detections occur with simultaneous LFQPO detections, such as the 5.8 Hz QPO for the type A PDS and the 6.4 Hz QPO for type B PDS in XTE J1550−564 shown in Figure 1. In the case of GRO J1655−40, there is more than one LFQPO present in some observations (Remillard et al. 1999b), and we select the QPO at 12.2–17.5 Hz that is very strong in the highest energy band, since it is present in all of the observations that exhibit the HFQPO at either 300 or 450 Hz. We have examined all of the coordinate frequencies and their beat frequencies at the resonance radii consistent with the HFQPOs in each of the two sources. We conclude that the 2 : 1 resonances, but not the 3 : 1 resonance, can possibly account for the observed LFQPO frequencies as a beat between the orbital

and polar coordinate frequencies. This beat frequency is a precession known as "frame dragging" (e.g., Merloni et al. 1999). In the top panels of Figure 8 the regions shaded with darker blue show the subset of resonance parameters for XTE J1550−564 in which the frame-dragging frequency lies in the range 5.8–6.4 Hz. Similarly for GRO J1655−40, in the bottom panels of Figure 8, the darker blue region shows black hole parameters for which the frame dragging frequency is in the range 12.2–17.5 Hz. We caution that the identification of particular LFQPO features with relativistic frame dragging is, at this point, highly speculative.

Thus far, there is no detailed description as to how a resonance between coordinate frequencies in GR could produce the requisite X-ray oscillations and the alternating conditions that cause the second or third harmonic to become the dominant QPO. Another challenging problem is the evidence for frequency jitter in the HFQPOs of XTE J1550−564. Because the radial dependence of the two relevant coordinate frequencies is so different, the resonances must be confined to a narrow range in radius. This is a particular problem for the 3 : 1 resonance, where the ratio of the orbital to radial coordinate frequencies changes rapidly with radius. We illustrate the diverging orbital and radial coordinate frequencies in Figure 9. In the top panel we show the radius that would yield a 3 : 1 resonance at 276 : 92 Hz for the case of a 10 $M_\odot$ black hole with $a_* = 0.465$. This illustrates a point in the blue-shaded region in the upper left-hand panel of Figure 8, and the resonance occurs at $5.03r_g$. Here a shift in the orbital frequency by $\pm 10\%$ implies that the radius must vary between $4.7R_g$ and $5.4r_g$, and the ratio of coordinate frequencies would then vary in the range 2.5–4.1. It may then be impossible to shift the radius of the perturbation enough to match the shifted HFQPOs and yet maintain the perturbation (no longer in resonance) throughout an *RXTE* observation, which is longer than the dynamical time by a factor of $\sim 10^6$. The problem is less serious, but nontrivial, for the 2 : 1 resonance, as shown in the bottom panel of Figure 9. For the same black hole mass and $a_* = 0.324$ (consistent with a 184 : 92 Hz resonance at 6.72 r_g), a 10% frequency shift corresponds to a range of radii of 6.3–7.2 r_g, over which the ratio of coordinate frequencies changes by about $\pm 20\%$. These considerations challenge the concept of resonance only in its most literal sense (i.e., matter buildup at discrete radii).

Finally, we note that all of the QPO models suffer from the ongoing uncertainty as to the origin and geometry of the X-ray power-law component, widely attributed to inverse Compton scattering of thermal photons. We cannot posit a simple way in which the resonance model can appear to shift harmonics in response to increased Comptonization.

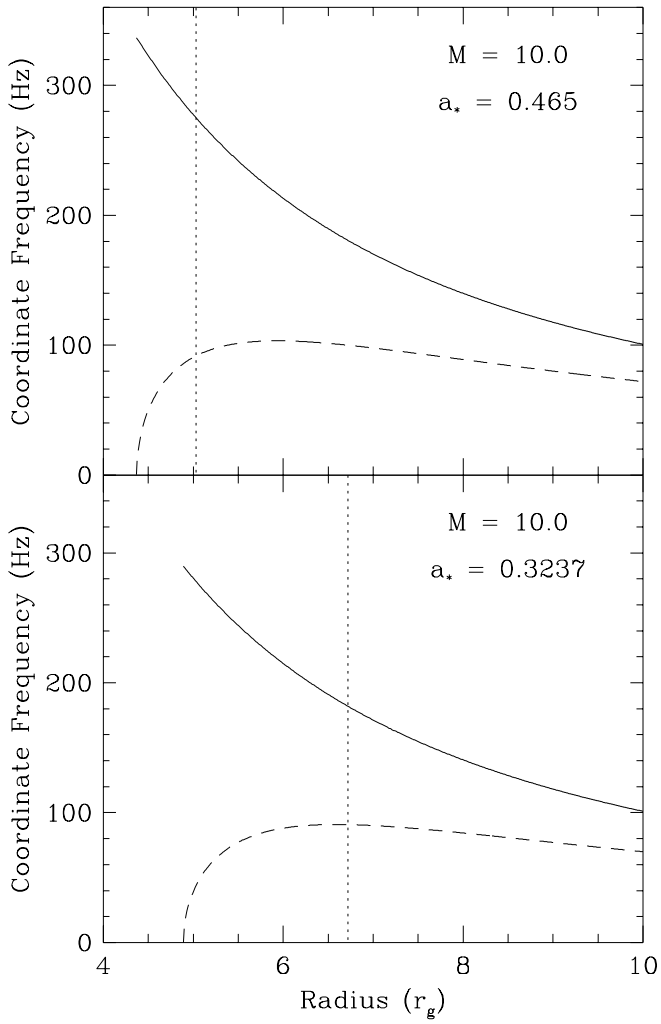

FIG. 9.—Frequencies predicted by GR as a function of radius, for cases that illustrate a 3 : 1 resonance (*top*) and a 2 : 1 resonance (*bottom*) between the orbital (*solid curve*) and radial (*dashed curve*) coordinate frequencies. In each case the mass is 10 $M_\odot$ and the spin parameter has been chosen to match the resonances to the values 276 : 92 Hz and 184 : 92 Hz, respectively. The different gradients in the coordinate frequencies create a narrow region in radius where the frequency ratio is near an integral value. Shifts in the observed frequencies may therefore be very difficult to accommodate in the resonance model, especially for the 3 : 1 resonance.

4.2. *Diskoseismic Oscillation Models*

A different model that warrants consideration with respect to harmonic HFQPOs in black hole binaries is the diskoseismic model (Kato & Fukue 1980; Wagoner 1999; Kato 2001; Wagoner et al. 2001). Here GR theory predicts that the inner accretion disk may trap oscillations, which is a consequence related to the turnover in the radial coordinate frequency at small radii, which was noted previously. The concept of a resonance cavity in the inner disk is naturally attractive with respect to our interpretation of harmonically related HFQPOs. The three-dimensional character of the model allows for modest shifts in oscillation frequency, e.g., with changes in disk thickness and luminosity (Wagoner 1999). Such changes in disk conditions would, in principle, produce coupled changes in both the X-ray spectrum and the oscillation frequency.

The strongest oscillations are expected to arise from gravity modes ("g-modes"), which were investigated in Kerr geometry by Perez et al. (1997). For adiabatic perturbations, the eigenfunction solution predicts a fundamental radial mode ($m = 0$) that would be in the range ~70–110 Hz for a 10 $M_\odot$ black hole with $0 < a_* < 0.5$. However, for higher m-number, the g-mode frequencies do not increase by integral values (Perez et al. 1997), and so the predictions do not match the observed HFQPO frequencies. It was noted that the ratio of the orbital frequency at the inner disk radius to the fundamental g-mode frequency is close to a value of 3.08 for a wide range in a_* (Wagoner 1999). However, the prediction for a strong feature at ν and a weak feature near 3ν does not resemble the observations.

Investigations have also been made for diskoseismic *p*-modes (Ortega-Rodriguez & Wagoner 2000) and *c*-modes (Silbergleit, Wagoner, & Ortega-Rodriguez 2001), but neither study predicts a system of linear harmonics. Kato (2001) has pointed out that the results of numerical simulations and eigenmode analyses show some differences, and therefore further study is warranted. Clearly, there is also a need to investigate the possibility of resonances within the paradigm of diskoseismology.

Partial support for R. R. and M. M. was provided by the NASA contract to MIT for *RXTE* instruments. J. M. acknowledges the support of NASA grant NAG 5-10813. Radleigh Santos helped to process *RXTE* data for the 2000 outburst of XTE J1550−564. We thank Michiel van der Klis, Al Levine, Tomasso Belloni, Wlodek Kluzniak, and Marek Abramowicz for providing very helpful comments.

REFERENCES

Abramowicz, M. A., & Kluzniak, W. 2001, A&A, 374, L19
Belloni, T., Psaltis, D., & van der Klis 2002, ApJ, 572, 392
Corbel, S., et al. 2001, ApJ, 554, 43
Greene, J., Bailyn, C. D., & Orosz, J. A. 2001, ApJ, 554, 1290
Hannikainen, D., et al. 2001, Ap&SS, 276, 45
Homan, J., Wijnands, R., van der Klis, M., Belloni, T., van Paradijs, J., Klein-Wolt, M., Fender, R., & Méndez, M. 2001, ApJS, 132, 377
Jain, R., Bailyn, C. D., Orosz, J. A., McClintock, J. E., Sobczak, G. J., & Remillard, R. A. 2001, ApJ, 546, 1086
Kalemci, E., Tomsick, J. A., Rothschild, R. E., Pottschmidt, K., & Kaaret, P. 2001, ApJ, 563, 239
Kato, S. 2001, PASJ, 53, 1
Kato, S., & Fukue, J. 1980, PASJ, 32, 377
Leahy, D., Darbro, W., Weisskopf, M. C., Kahn, S., Sutherland, P. G., & Grindlay, J. E. 1983, ApJ, 266, 160
Merloni, A., Vietri, M., Stella, L., & Bini, D. 1999, MNRAS, 304, 155
Miller, J. M., et al. 2001, ApJ, 563, 928
Morgan, E. H., Remillard, R. A., & Greiner, J. 1997, ApJ, 482, 993
Muno, M. P., Morgan, E. H., & Remillard, R. A. 1999, ApJ, 527, 321
Nowak, M. 2000, MNRAS, 318, 361
Orosz, J. A., et al. 2002, ApJ, 568, 845
Ortega-Rodriguez, M., & Wagoner, R. V. 2000, ApJ, 543, 1060
Perez, C.A., Silbergleit, A. S., Wagoner, R. V., & Lehr, D. E. 1997, ApJ, 476, 589
Pottschmidt, K., et al. 2002, A&A, submitted (astro-ph/0202258)
Psaltis, D., Belloni, T., & van der Klis, M. 1999, ApJ, 520, 262
Remillard, R. A., McClintock, J. E., Sobczak, G. J., Bailyn, C. D., Orosz, J. A., Morgan, E. H., & Levine, A. M. 1999a, ApJ, 517, L127
Remillard, R. A., Morgan, E. H., McClintock, Bailyn, C. D., & Orosz, J. A. 1999b, ApJ, 522, 397
Remillard, R. A., Sobczak, G. J., Muno, M., & McClintock, J. E. 2002, ApJ, 564, 962
Revnivtsev, M., Gilfanov, M., & Churazov, E. 2000, A&A, 363, 1013
Shahbaz, T., et al. 1999, MNRAS, 306, 89
Shapiro, S. L., & Teukolsky, S. A. 1983, Black Holes,White Dwarfs, and Neutron Stars (New York: Wiley)
Silbergleit, A. S., Wagoner, R. V., & Ortega-Rodriguez, M. 2001, ApJ, 548, 335
Sobczak, G. J., McClintock, J. E., Remillard, R. A., Bailyn, C. D., & Orosz, J. A. 1999, ApJ, 520, 776
Sobczak, G. J., McClintock, J. E., Remillard, R. A., Cui, W., Levine, A. M., Morgan, E. H., Orosz, J. A., & Bailyn, C. D. 2000a, ApJ, 531, 537
Sobczak, G. J., et al. 2000b, ApJ, 544, 993
Strohmayer, T. E. 2001a, ApJ, 552, L49
———. 2001b, ApJ, 554, L169
Swank, J., Smith, E., & Markwardt, C. 2002, IAU Circ. 7792
Tomsick, J. A., Corbel, S., & Kaaret, P. 2001, ApJ, 563, 229
Tomsick, J. A., Smith, D. A., Swank, J. H., Wijnands, R., & Homan, J. 2001, IAU Circ. 7575
Wagoner, R. V. 1999, Phys. Rep., 311, 259
Wagoner, R. V., Silbergleit, A. S., & Ortega-Rodriguez, M. 2001, ApJ, 559, L25
Wijnands, R., Homan, J., & van der Klis, M. 1999, ApJ, 526, 33
Zhang, S. N., Cui, W., & Chen, W. 1997, ApJ, 482, L155